Published in final edited form as:
J Nucl Med. 2011 September ; 52(9): 1339–1345. doi:10.2967/jnumed.111.091587.

Human Dosimetry and Preliminary Tumor Distribution of ^{18}F-Fluoropaclitaxel in Healthy Volunteers and Newly Diagnosed Breast Cancer Patients Using PET/CT

Karen A. Kurdziel[1], **Joseph D. Kalen**[2], **Jerry I. Hirsch**[3], **John D. Wilson**[3], **Harry D. Bear**[4], **Jean Logan**[5], **James McCumisky**[3], **Kathy Moorman-Sykes**[3], **Stephen Adler**[6], and **Peter L. Choyke**[1]

[1]Molecular Imaging Program, Center for Cancer Research/National Cancer Institute/National Institutes of Health, Bethesda, Maryland [2]Small Animal Imaging Program, Laboratory Animal Sciences Program, SAIC-Frederick, Inc., Frederick, Maryland [3]Department of Radiology, Virginia Commonwealth University, Richmond, Virginia [4]Department of Surgery and the Massey Cancer Center, Virginia Commonwealth University, Richmond, Virginia [5]Medical Department, Brookhaven National Laboratory, Upton, New York [6]SAIC Fredrick-Inc., Contractor to Molecular Imaging Program, NCI, Fort Detrick, Frederick, Maryland

Abstract

^{18}F-fluoropaclitaxel is a radiolabeled form of paclitaxel, a widely used chemotherapy agent. Preclinical data suggest that ^{18}F-fluoropaclitaxel may be a reasonable surrogate for measuring the uptake of paclitaxel. As a substrate of P-glycoprotein, a drug efflux pump associated with multidrug resistance, ^{18}F-fluoropaclitaxel may also be useful in identifying multidrug resistance and predicting tumor response for drugs other than paclitaxel.

Methods—After informed consent was obtained, 3 healthy volunteers and 3 patients with untreated breast cancer (neoadjuvant chemotherapy candidates, tumor size > 2 cm) received an intravenous infusion of ^{18}F-fluoropaclitaxel and then underwent PET/CT. Healthy volunteers underwent serial whole-body imaging over an approximately 3-h interval, and organ ^{18}F residence times were determined from the time–activity curves uncorrected for decay to determine dosimetry. Radiation dose estimates were calculated using OLINDA/EXM software. For breast cancer patients, dynamic imaging of the primary tumor was performed for 60 min, followed by static whole-body scans at 1 and 2 h after injection.

Results—Dosimetry calculations showed that the gallbladder received the highest dose (229.50 μGy/MBq [0.849 rad/mCi]), followed by the small and large intestines (161.26 μGy/MBq [0.597 rad/mCi] and 184.59 μGy/MBq [0.683 rad/mCi]). The resultant effective dose was 28.79 μGy/MBq (0.107 rem/mCi). At approximately 1 h after injection, an average of 42% of the decay-corrected activity was in the gastrointestinal system, with a mean of 0.01% in the tumor. All 3 breast cancer patients showed retention of ^{18}F-fluoropaclitaxel and ultimately demonstrated a complete pathologic response (no invasive cancer in the breast or axillary nodes) to chemotherapy that included a taxane (either paclitaxel or docetaxel) at surgical resection. The tumor-to-background ratio increased with time to a maximum of 7.7 at 20 min.

For correspondence or reprints contact: Karen A. Kurdziel, National Cancer Institute/National Institutes of Health, 10 Center Dr., Room B3B403, Bethesda, MD 20892. kurdziek@mail.nih.gov.

Disclosure Statement: The costs of publication of this article were defrayed in part by the payment of page charges. Therefore, and solely to indicate this fact, this article is hereby marked “advertisement” in accordance with 18 USC section 1734.

Conclusion—This study demonstrates the feasibility of using ^{18}F-fluoropaclitaxel PET/CT tumor imaging and provides radiation dosimetry measurements in humans. Although further study is needed, it is hoped that the measured intratumoral ^{18}F-fluoropaclitaxel distribution can serve as a surrogate for paclitaxel, and potentially other chemotherapeutic agent retention, in solid tumors.

Keywords

^{18}F-fluoropaclitaxel (FPAC); multidrug resistance (MDR); PET/CT imaging; paclitaxel; dosimetry; breast cancer

---

The cause of chemotherapeutic failure is multifactorial and may include insufficient drug delivery and retention. Traditional methods of assessing drug delivery rely on measuring plasma drug concentration to infer tumor drug concentration. However, the perfusion, and hence delivery of chemotherapeutic agents, in tumors has been shown to be quite heterogeneous and even varies over short periods of time. Drug penetration in solid tumors can be limited by factors such as high interstitial pressure, vascular heterogeneity, and regional necrotic foci, among others, limiting the validity of using plasma drug concentrations to evaluate tumor drug concentration. Once the active drug reaches the tumor cells, it may or may not reach sufficient concentrations to be effective, or once in the tumor cells, the drug may be removed by by membrane drug transporters. Multidrug resistance, in which tumors are resistant to a host of chemically dissimilar drugs, is a well-known phenomenon in oncology. Although the exact cause remains elusive, membrane proteins—which actively remove drugs from the intracellular compartment—are felt to play a role. The best characterized of these drug-resistance proteins is P-glycoprotein (Pgp), an adenosine triphosphate–binding cassette transporter, which transports substrates across the cell membrane against the concentration gradient. Pgp is normally expressed in the liver, kidney, intestine, blood– brain barrier (BBB), blood–testicular barrier, and hematopoietic stem cells, in which its function appears either to prevent toxins from accumulating in tissues (returning them to the bloodstream), as in the BBB, or to remove toxins from the body (extracting them from the bloodstream), as in the liver and kidney (1,2). Overexpression of Pgp is found in many drug-resistant tumors. With the intent of developing a radiolabeled drug that could be used to visualize drug distribution in vivo and measure changes in its uptake over time, a radiolabeled analog of paclitaxel, ^{18}F-fluoropaclitaxel, was developed by the PET department of the National Institutes of Health (3).

Paclitaxel, a naturally occurring taxane derived from the yew tree (*Taxus brevifolia*) (4), is a neutral tubulin-binding agent that is a widely used chemotherapeutic agent. Initial tumor delivery of paclitaxel is ostensibly dependent on tumor mitotic rate and perfusion, but drug efflux pumps may also play a role. Paclitaxel is a well-characterized Pgp substrate; therefore, monitoring the kinetics of its distribution may also provide insight into Pgp-dependent drug efflux and could potentially be predictive of tumor retention of other drugs that are Pgp substrates.

In vitro data have shown ^{18}F-fluoropaclitaxel and paclitaxel to have similar cytotoxicity (K.A. Kurdziel and C. Cardarelli, unpublished data, 2000). ^{18}F-fluoropaclitaxel biodistribution studies in mdr 1a/1b knockout and wild-type mice showed differences consistent with Pgp-dependent efflux. Coadministration of ^{3}H-paclitaxel and ^{18}F-paclitaxel gave similar biodistribution (3). A comparison of biodistribution of ^{18}F-fluoropaclitaxel in Pgp-expressing drug-sensitive and drug-resistant human tumor xenografts of breast (5) and other epithelial cell cancers (6) showed decreased ^{18}F-fluoropaclitaxel accumulation in the resistant tumors. A recent paper showed that in a mouse xenograft model, tumor uptake of ^{18}F-fluoropaclitaxel correlated with tumor response to treatment with paclitaxel (7).

Using a Pgp-specific modulator, XR9576 (Xenova Ltd.), we used ^{18}F-fluoropaclitaxel PET to obtain images in vivo and quantify Pgp inhibition in normal tissues of rhesus monkeys (8).

On the basis of preclinical data and using radiation dose estimates from nonhuman primates, a pilot clinical investigation was conducted in healthy volunteers and breast cancer patients. This paper describes the first-in-human, to our knowledge, imaging characteristics, biodistribution, and dosimetry for ^{18}F-fluoropaclitaxel.

Materials and methods

^{18}F-Fluoropaclitaxel Synthesis

^{18}F-fluoropaclitaxel, MW 871, was synthesized by nucleophilic substitution, originally described by Kiesewetter et al. (3,9) using a modified automated radiochemical synthetic method on a dualreaction vessel synthesizer (TRACERlab FXF-N; GE Healthcare–Functional Imaging GmbH) as described by Kalen et al. (10) Appropriate controls were used to allow administration of the product in human pilot studies under an investigational new drug application. The final product specifications were 17.4% (v:v) ethanol and 82.6% (v:v), with a radiochemical purity of 95% or greater, and chemical purity (by high-performance liquid chromatography) of 7.3 ug/mL or less. The average chemical yield was approximately 21.2% ± 9.6%.

This study was approved by the local institutional review board and the Food and Drug Administration (investigation new drug 75855). Informed consent was obtained from all participants. The study population included 3 healthy volunteers (2 women and 1 man) and 3 untreated female breast cancer patients with mean CT tumor volumes of 18.7 mL, who were candidates for neoadjuvant chemotherapy before definitive surgery (resection of the primary and axillary evaluation by sentinel node biopsies). Two women had segmental mastectomies and 1 had a total mastectomy. All subjects underwent an intravenous infusion of ^{18}F-fluoropaclitaxel (mean, 192.4 MBq [5.2 mCi]; range, 99.9–277.5 MBq [2.7–7.5 mCi], and mean chemical mass dose, 2.5 μg [range, 0.6–6.9 μg]) over approximately 30 s. The average specific activity at the end of synthesis was 127.502 TBq/mmol (3,446 Ci/mmol; range, 16.65–237.91 TBq/mmol [450–6,430 Ci/mmol]). Throughout the imaging protocol, the subjects underwent interval monitoring of heart rate, blood pressure, pulse oxymetry, and heart rhythm and were queried for potential adverse events.

Healthy Volunteers

The healthy volunteers underwent transmission CT (140 keV, 68 mA, 512 × 512), followed by sequential whole-body (vertex to upper thighs) imaging, at 2 min/bed position, for approximately 60–85 min (dependent on patient size) on a Light Speed Discovery PET scanner (GE Healthcare) in 2-dimensional mode. Additional static wholebody PET/CT images were obtained at 2 and 3 h after tracer injection.

Breast Cancer Patients

The 3 breast cancer patients underwent 60 min of dynamic imaging over a single bed position, with the primary lesion in the field of view, immediately followed by a whole-body static emission scan. To assess the changes in ^{18}F-fluoropaclitaxel tumor distribution over time, an additional whole-body static emission scan was obtained at approximately 3 h after injection. Corresponding low-dose transmission scans were also acquired.

Each patient subsequently underwent standard-of-care neoadjuvant chemotherapy, followed by surgery with curative intent, and pathologic response data were obtained. One patient

received paclitaxel plus trastuzumab, followed by doxorubicin plus cyclophosphamide (AC); another received paclitaxel plus carboplatin plus trastuzumab; and the third received docetaxel plus gemcitabine followed by AC. When available, clinical ^{18}F-FDG PET/CT scans were also evaluated.

Data Analysis

For the solid organs (brain, muscle, lung, myocardium, bone marrow [represented by a vertebral body], spleen, renal cortex, and liver) and the blood input function, uncorrected for metabolites (estimated from heart, or nearby large vessel if the heart was not in the field of view), a small representative volume of interest (VOI) was drawn in a homogeneous region using both the transmission CT and PET images for accurate localization. For the hollow organs (gallbladder, gut, and urinary bladder), a VOI encompassing the entire organ (including regions in which the counts spilled outside the true anatomic boundaries) was drawn. Care was taken to avoid VOI overlap. Separate sets of VOIs were created for each PET/CT image pair (i.e., 1 set was drawn for the sequential whole-body images, which were registered to the initial transmission CT), and an additional set was drawn for each of the static whole-body images. The VOIs were applied to both the decay-corrected and non–decay-corrected images at each imaging time point, and time–activity curves were generated.

Dosimetry

Dosimetry estimates were performed using the normal organ data collected from the healthy volunteers. The total activity within the hollow organs was obtained by multiplying the mean activity (Bq/mL) by the VOI (mL). Using the non–decay-corrected time–activity curves, we integrated these values over the entire imaging period and normalized the values to the injected dose to obtain organ ^{18}F residence times. The measured fraction of activity entering the small bowel (approximated by the total measured gastrointestinal activity residence times) for the lower large intestine, upper large intestine, and small intestine were obtained using the gastrointestinal model of the International Commission on Radiological Protection.

Residence times for the solid organs were obtained by integrating the mean VOI activity concentration over the imaging period, normalizing to the injected activity, and then multiplying by the respective standard man (70 kg) organ density and organ weights. Mean radiation dose estimates (n = 3) were obtained using OLINDA/EXM software, which was granted a 510(k)-K03396 by the U.S. Food and Drug Administration as a software device (11).

Tumor and Normal-Tissue Biodistribution

Standardized uptake value (SUV) time–activity curves were created for each organ and the tumors (when present) on the decay-corrected image sets. The time–activity curves were evaluated using a graphical analysis for reversible tracers (12), with the slope estimating the distribution volume ratio, which is a linear function of receptor availability, and Patlak graphical analysis (13), with the slope representing the tracer influx constant. Cumulative activity or concentration intervals were also derived.

Results

Adverse Events

Of the 6 subjects injected with ^{18}F-fluoropaclitaxel, only grade 1 transitory pain or burning on injection was noted in the first subject. Decreasing the infusion rate and increasing the injectate volume with saline dilution in subsequent subjects resulted in no further adverse

events. There were no clinically significant changes in vital signs, lead II electrocardiogram, blood chemistry, or complete blood counts between baseline and postinjection samples.

Normal-Organ Biodistribution

The PET images revealed rapid uptake of ^{18}F-fluoropacli-taxel into the liver, followed by excretion into the gastrointestinal tract. Excretion by the kidneys was low relative to the liver and gastrointestinal tract: cumulative gastrointestinal tract and urinary bladder activity were estimated at 46% and 3.2% of the whole-body activity, respectively. The uptake in the brain was negligible, consistent with the expected exclusion of ^{18}F-fluoropaclitaxel by the BBB. A small focus of uptake was noted in the pituitary, which is not protected by the BBB. Figure 1 shows organ distribution in a representative healthy volunteer at several time points. Mean time–activity curves for selected solid organs are shown in Figure 2.

Dosimetry

Human dose estimates were obtained using the methodology described in the “Materials and Methods” section. The fraction of radioactivity entering the small bowel was approximately 0.46, which was the value used in the International Commission on Radiological Protection gastrointestinal model in OLINDA. The organ receiving the highest radiation dose was the gallbladder, followed by the large intestine and small intestine at 229.50, 184.59, and 161.26 μGy/MBq (0.849, 0.683, and 0.597 rad/mCi), respectively. The effective dose was 28.79 μSv/MBq (0.107 rem/mCi). Table 1 lists the mean radiation dosimetry estimates and SD from the 3 healthy volunteers. The breast cancer patient data were not used in the dosimetry calculations.

Tumor Uptake

The absolute tumor uptake was low (average maximum SUV [SUV_{max}], 1.8, with an average tumor time–activity curve peaking at 80 s after injection), with a slight decrease over time (Fig. 3). When compared with background tissue (contralateral breast), the tumors were visible, with an average tumor-to-background time–activity curve peak of 7.7 at 20 min. Tumor–to–blood-pool ratios appeared to rise slightly over time to an average maximum of 1.9, suggesting a slow or irreversible component; however, the Patlak analysis–estimated net rates of tracer influx into the tumor (K_i) were quite low (all < 0.006 mL/cm^3/min). The tumor kinetics fit the reversible graphical analysis using a reference region with tumor distribution volume ratio of 3.8, 9.4, and 3.7 for patients FPAC2001, FPAC2002, and FPAC2003, respectively, becoming linear at approximately 10 min (Fig. 4). At 1 h after injection, the average amount of ^{18}F-fluoropaclitaxel in the tumors was 0.01% of the administered dose, whereas an estimated 42% of the administered dose was retained in the gastrointestinal system.

Clinical ^{18}F-FDG baseline studies were available for all 3 patients. The ^{18}F-FDG tumor SUVs were much higher than those of ^{18}F-fluoropaclitaxel, as seen in Figure 5, which displays representative patient images, including ^{18}F-fluoropaclitaxel, ^{18}F-FDG, and coregistered CT. All 3 patients had a complete pathologic response (defined as no invasive cancer in the breast or axillary sentinel lymph nodes) at surgery following neoadjuvant therapy. One patient had hilar mediastinal ^{18}F-FDG uptake, showing no corresponding increased ^{18}F-fluoropaclitaxel uptake (Fig. 6). A biopsy revealed sarcoidosis.

Discussion

In this study, ^{18}F-fluoropaclitaxel PET/CT was performed in 6 subjects without significant adverse events. The ^{18}F was eliminated from the blood rapidly, mostly through the liver and gastrointestinal tract, with a minor component excreted through the kidneys. Radiation

dosimetry estimates show that the organ receiving the highest radiation dose was the gallbladder, followed by the upper large intestine and small intestine at 229.50, 184.59, and 0.597 μGy/MBq (0.849, 0.683, and 0.597 rad/mCi), respectively. The effective dose was 28.79 μSv/MBq (0.107 rem/mCi) (Table 1). The overall biodistribution and dose estimates were similar to those found in nonhuman primates; however, the dose to the liver was lower in humans (140.72 μGy/MBq [0.523 rad/mCi], nonhuman, vs. 40.23 μGy/MBq [0.149 rad/mCi], human). Dosimetry for an approximately 185- to 259-MBq (5- to 7-mCi) injection of ^{18}F-fluoropaclitaxel is comparable to other clinical imaging studies and was sufficient for depicting tumor uptake. The overall biodistribution within the liver and bowel (Fig. 1) makes it unlikely that this radiotracer will be useful for imaging below the diaphragm. However, the extremely low background above the diaphragm allows for even a small amount of tumor uptake to be visualized. All 3 breast cancer patients imaged had large tumors, all with high ^{18}F-FDG uptake, as well as measurable ^{18}F-fluoropaclitaxel uptake.

The data show rapid but low tumor uptake (estimated at 0.01% of the administered dose). After the initial perfusion phase, the tumor ^{18}F-fluoropaclitaxel retention was essentially constant and the tumor-to-background ratio increased with time, suggesting some degree of tumor-specific retention. Although the tumor-to-blood ratio appeared to rise slightly over time, suggesting an irreversible component, the estimated K_i from the Patlak analysis was low. The data fit well to a reversible reference region graphical analysis (Fig. 3), suggesting that the primary kinetics were reversible.

All 3 of the breast cancer patients showed complete pathologic responses to multidrug chemotherapy including a taxane. The kinetics of the tumor radioactivity after ^{18}F-fluoropaclitaxel injection were measurable. It is anticipated that ^{18}F-fluoropaclitaxel PET can serve as a surrogate for paclitaxel tumor uptake in solid tumors.

There are some limitations to predicting paclitaxel concentration estimates using ^{18}F-fluoropaclitaxel PET. The PET data represent a combination of both metabolized and unmetabolized ^{18}F-fluoropaclitaxel, inducing error in the tumor ^{18}F-fluoropaclitaxel concentration estimates. Although metabolites were not measured in this study, data from the previous nonhuman primate study (8) show that the percentage of ^{18}F activity representing metabolites increases with time but that more than 85% of the dose is still in the parent form for the first 20 min. Data acquired soon after injection are not expected to have a high metabolite fraction, and there is no reason to expect specific accumulation of radiolabeled metabolites in the tumor. Because the peak uptake of ^{18}F-fluoropaclitaxel occurs early, early imaging is feasible and would limit the contribution of metabolites to the resultant measurements.

An additional challenge to estimating therapeutic paclitaxel distribution using a tracer dose of ^{18}F-fluoropaclitaxel is the known nonlinear kinetics of paclitaxel (14). Because paclitaxel has been used extensively over the years, the kinetics in blood have been well studied. Henningsson et al. devised a method for modeling paclitaxel kinetics based on total blood concentration alone (15). It is expected that by combining ^{18}F-fluoropaclitaxel PET data with the existing paclitaxel pharmacokinetic modeling data, a more accurate prediction of intratumoral drug distribution can be made. Further studies performed while the patient is receiving a therapeutic dose of paclitaxel will also help improve the extrapolation of drug concentration from a tracer to a therapeutic dose.

^{18}F-fluoropaclitaxel PET may have potential utility beyond estimating intratumoral paclitaxel distributions. Because ^{18}F-fluoropaclitaxel is a substrate of Pgp—a membrane pump whose overexpression has been shown to result in multidrug resistance (3,5,6,8)—^{18}F-fluoropaclitaxel PET/CT may also serve as a good surrogate for tumor cell Pgp

function and multidrug resistance. Although further study is needed, the ability to predict which tumors actively eliminate, and thus may be resistant to, a wide range of chemotherapeutic drugs is a potential clinical application.

With the increasing interest in the use of adjunctive drugs such as antivascular or antiangiogenic agents, which may normalize blood flow to tumors (thus potentially enhancing delivery of a cytotoxic agent), a method for imaging the efficacy of such therapies is of interest. By estimating intratumoral delivery of paclitaxel, a chemotherapeutic agent, ^{18}F-fluoropaclitaxel PET may prove useful in this arena. Numerous mathematic models have been developed for estimating drug delivery in solid tumors; it is hoped that data obtained from ^{18}F-fluoropaclitaxel PET may be used to validate and improve such models.

Conclusion

This study demonstrates the feasibility of using ^{18}F-fluoropaclitaxel PET/CT to image tumors and provides the first, to our knowledge, radiation dosimetry measurements in humans. Because of the low accumulation of ^{18}F-fluoro-paclitaxel, initial tumor detection with this imaging agent is not likely. However, although further study is needed, it is anticipated that the measured intratumoral ^{18}F-fluoropacli-taxel distribution can serve as a surrogate for uptake of paclitaxel, and potentially other chemotherapeutic agents, in solid tumors.

Acknowledgments

We thank William C. Eckelman for preliminary review of this manuscript. This work was funded in part by the American Cancer Society, IRG-100036, and NCI, 1R21 CA098334-01A1. No other potential conflict of interest relevant to this article was reported.

References

1. Lum B, Gosland M. MDR expression in normal-tissues: pharmacological implications for the clinical use of P-glycoprotein inhibitors. Hematol Oncol Clin North Am. 1995; 9:319–336. [PubMed: 7642466]
2. Pavelic ZP, Reising J, Pavelic L, Kelley DJ, Stambrook PJ, Gluckman JL. Detection of P-glycoprotein with 4 monoclonal-antibodies in normal and tumor-tissues. Arch Otolaryngol Head Neck Surg. 1993; 119:753–757. [PubMed: 8100425]
3. Kiesewetter DO, Jagoda EM, Kao CH, et al. Fluoro-, bromo-, and iodopaclitaxel derivatives: synthesis and biological evaluation. Nucl Med Biol. 2003; 30:11–24. [PubMed: 12493538]
4. Sparreboom A, van Tellingen O, Nooijen WJ, Beijnen JH. Preclinical pharma-cokinetics of paclitaxel and docetaxel. Anticancer Drugs. 1998; 9:1–17. [PubMed: 9491787]
5. Gangloff A, Hsueh WA, Kesner AL, et al. Estimation of paclitaxel biodistribution and uptake in human-derived xenografts in vivo with ^{18}F-fluoropaclitaxel. J Nucl Med. 2005; 46:1866–1871. [PubMed: 16269601]
6. Kurdziel KA, Kiesewetter DO. PET imaging of multidrug resistance in tumors using ^{18}F-fluoropaclitaxel. Curr Top Med Chem. 2010; 10:1792–1798. [PubMed: 20645913]
7. Hsueh WA, Kesner AL, Gangloff A, et al. Predicting chemotherapy response to paclitaxel with ^{18}F-fluoropaclitaxel and PET. J Nucl Med. 2006; 47:1995–1999. [PubMed: 17138742]
8. Kurdziel K, Kiesewetter DO, Carson RE, Eckelman WC, Herscovitch P. Bio-distribution, radiation dose estimates, and in vivo pgp modulation studies of ^{18}F-paclitaxel in nonhuman primates. J Nucl Med. 2003; 44:1330–1339. [PubMed: 12902425]
9. Kiesewetter D, Eckelman W. Radiochemical synthesis of [18F]fluoropaclitaxel ([18F]FPAC). J Labelled Cpd Radiopharm. 2001; 44(suppl):S903–S905.

10. Kalen JD, Hirsch JI, Kurdziel KA, Eckelman WC, Kiesewetter DO. Automated synthesis of ^{18}F analogue of paclitaxel (PAC): [^{18}F]Paclitaxel (FPAC). Appl Radiat Isot. 2007; 65:696–700. [PubMed: 17161952]

11. Stabin MG, Sparks RB, Crowe E. OLINDA/EXM: the second-generation personal computer software for internal dose assessment in nuclear medicine. J Nucl Med. 2005; 46:1023–1027. [PubMed: 15937315]

12. Logan J, Fowler JS, Volkow ND, Wang GJ, Ding YS, Alexoff DL. Distribution volume ratios without blood sampling from graphical analysis of PET data. J Cereb Blood Flow Metab. 1996; 16:834–840. [PubMed: 8784228]

13. Patlak CS, Blasberg RG. Graphical evaluation of blood-to-brain transfer constants from multiple-time uptake data. Generalizations. J Cereb Blood Flow Metab. 1985; 5:584–590. [PubMed: 4055928]

14. Tamura T, Sasaki Y, Nishiwaki Y, Saijo N. Phase I study of paclitaxel by three-hour infusion: hypotension just after infusion is one of the major dose-limiting toxicities. Jpn J Cancer Res. 1995; 86:1203–1209. [PubMed: 8636011]

15. Henningsson A, Karlsson MO, Vigano L, Gianni L, Verweij J, Sparreboom A. Mechanism-based pharmacokinetic model for paclitaxel. J Clin Oncol. 2001; 19:4065–4073. [PubMed: 11600609]

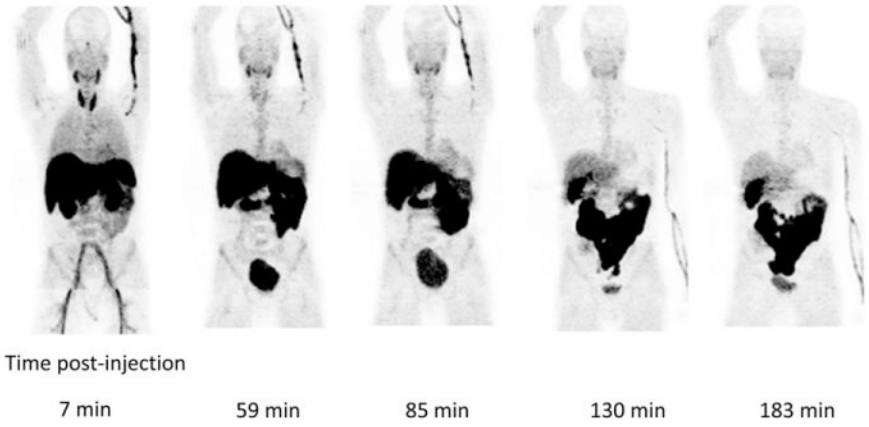

FIGURE 1.
Serial coronal maximum-intensity-projection images of healthy volunteer after left wrist injection of 218.3 MBq (5.9 mCi) of ^{18}F-fluoropaclitaxel.

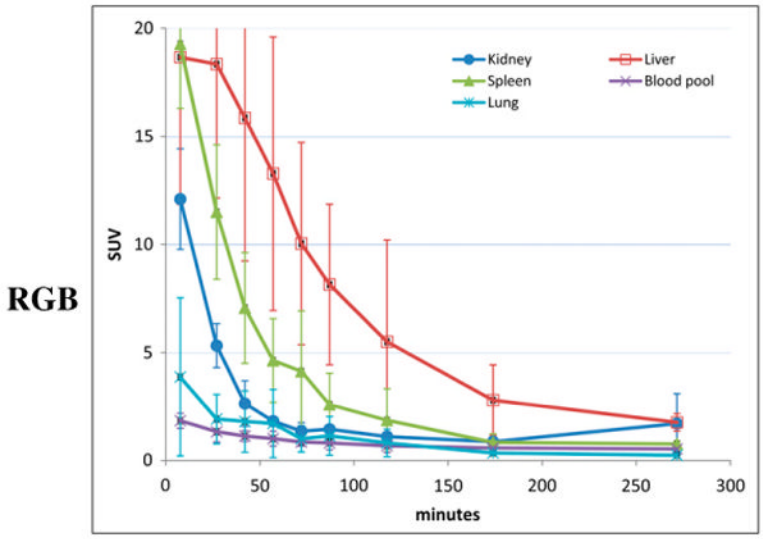

FIGURE 2.
Average time–activity curves for selected solid organs in 3 healthy volunteers. Error bars represent SD.

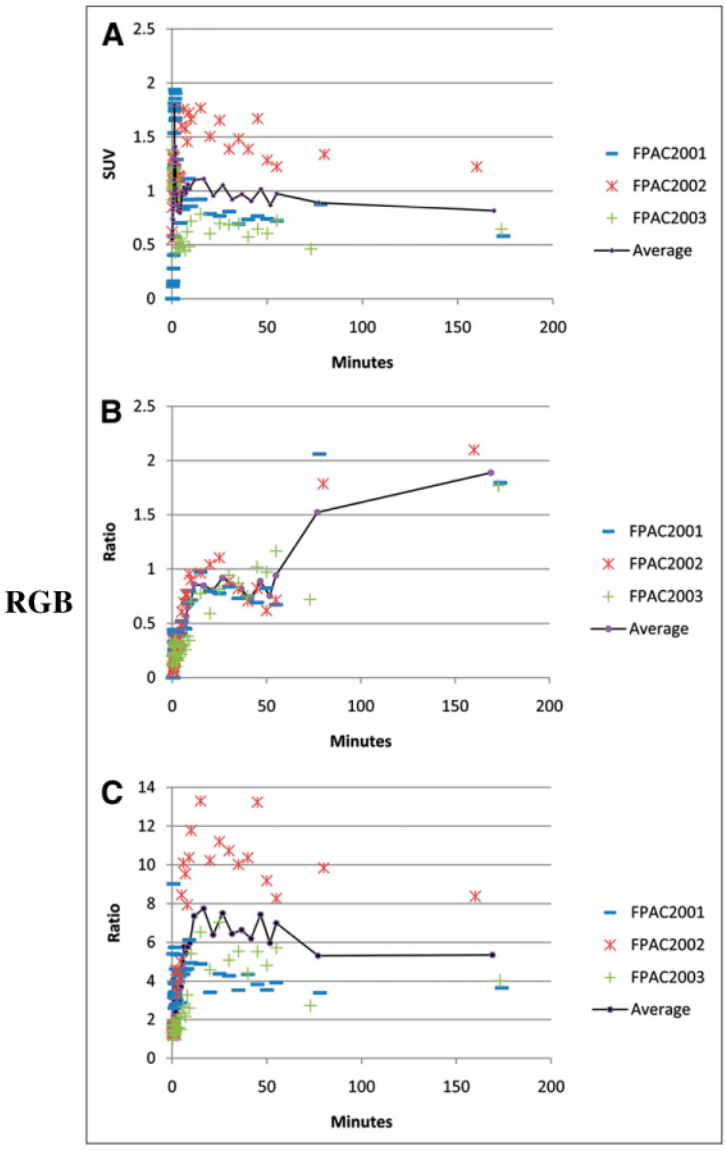

FIGURE 3.
Time–activity curves for tumor SUV (A), tumor to blood pool (B), and tumor to background (C).

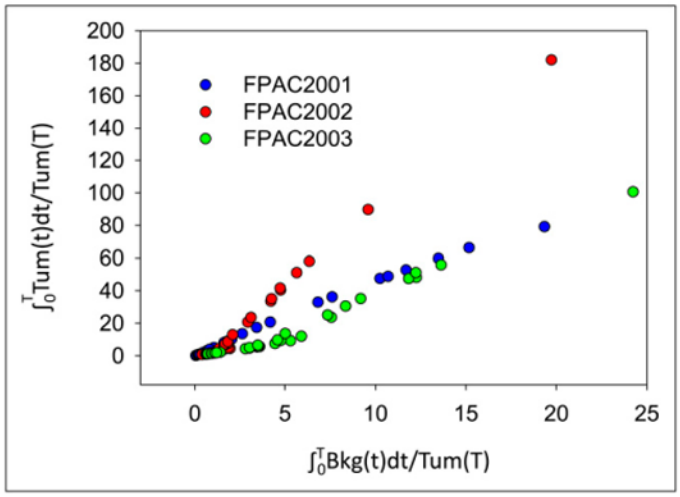

FIGURE 4.
Graphical analysis of dynamic tumor data for all 3 patients. Slope of linear portion estimates distribution volume ratio of tumor and reference tissue (in this case, contralateral noninvolved breast).

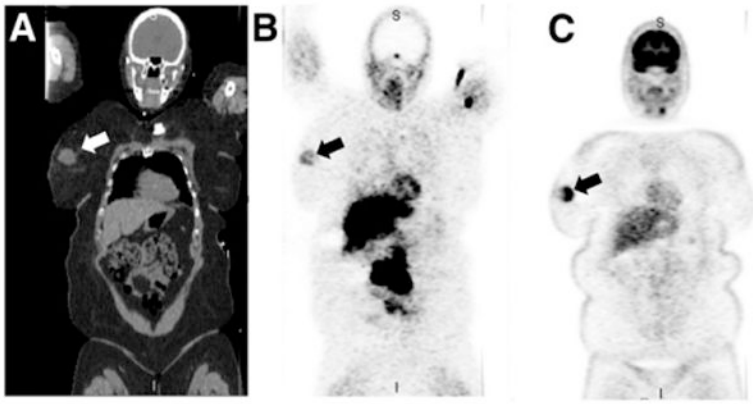

FIGURE 5.
Coregistered coronal CT (A), ^{18}F-fluoropaclitaxel (SUV_{max}, 1.2) (B), and ^{18}F-FDG (SUV_{max}, 12.0) (C) maximum-intensity-projection images of breast cancer patient with large right confirmed breast tumor (arrow).

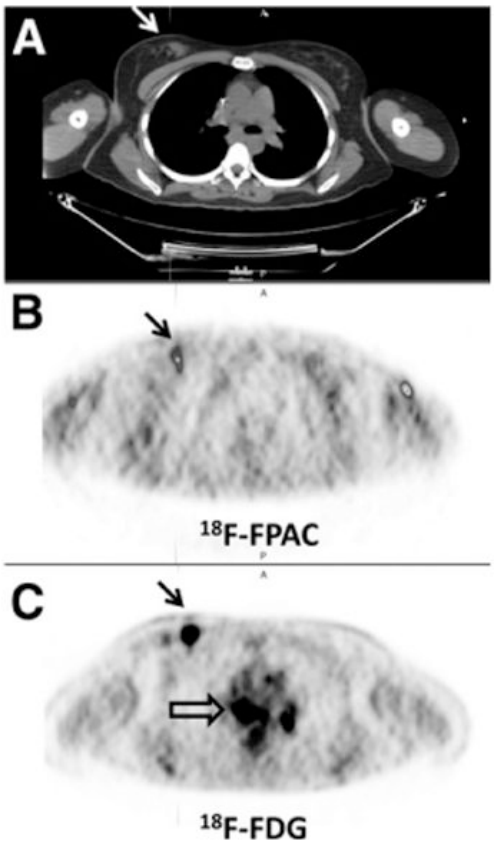

FIGURE 6.

Breast cancer patient with biopsy-proven tumor in right breast mass (arrows on CT [A] and PET [B and C] scans) and biopsy-proven sarcoid in mediastinum or hila. Increased ^{18}F-fluoropacli-taxel (B; SUV uptake corresponding to tumor and no ^{18}F-fluoropaclitaxel uptake corresponding to mediastinum/hilar lesions) seen on ^{18}F-FDG scan (C; open arrow). ^{18}F-FDG and ^{18}F-fluoropaclitaxel images are scaled to SUV_{max} of 2.0. Tumor SUV_{max} on^{18}F-fluoropa-clitaxel (B) at 78 min was 0.9; ^{18}F-FDG (C) SUV_{max} at 123 min was 10.0. Uptake in anterior portion of left arm on ^{18}F-fluoropaclitaxel image (B) is residual tracer within vessel wall. FPAC 5 fluoropaclitaxel.

TABLE 1

Human Dose Estimates (n = 3)

Organ	Rad/mCi	μGy/MBq	SD
Adrenals	0.034	9.28	0.008
Brain	0.004	1.06	0.004
Breasts	0.008	2.29	0.003
Gallbladder	0.849	229.50	0.914
Lower large intestine	0.216	58.47	0.010
Small intestine	0.597	161.26	0.016
Stomach	0.066	17.74	0.021
Upper large intestine	0.683	184.59	0.016
Heart	0.033	8.82	0.021
Kidneys	0.076	20.66	0.020
Liver	0.149	40.23	0.085
Lungs	0.057	15.33	0.039
Muscle	0.025	6.70	0.004
Ovaries	0.106	28.74	0.007
Pancreas	0.045	12.03	0.003
Red marrow	0.082	22.04	0.072
Osteogenic cells	0.044	11.76	0.041
Skin	0.009	2.39	0.002
Spleen	0.072	19.44	0.033
Testes	0.008	2.20	0.002
Thymus	0.010	2.58	0.004
Thyroid	0.084	22.83	0.141
Urinary bladder	0.056	15.23	0.021
Uterus	0.079	21.24	0.004
Total body	0.036	9.69	0.006

Effective dose equivalent = 0.198 rem/mCi (53.51 μSv/MBq); effective dose = 0.107 rem/mCi (28.79 μSv/MBq).